Article

A Hybrid Active Damping Strategy for Improving the Adaptability of LCL Converter in Weak Grid

Jingtao Huang [1,2,*] , **Yiju Zhao** [1] , **Jie Wang** [1] **and Peng Zhang** [3]

1   College of Information Engineering, Henan University of Science and Technology, Luoyang 471023, China
2   Henan Engineering Laboratory of Power Electronic Devices and Systems, Luoyang 471023, China
3   China Railway Engineering Equipment Group Co., Ltd., Zhengzhou 450016, China
*   Correspondence: jthuang@haust.edu.cn

Abstract: In a weak grid, the line impedance variation will cause the resonant frequency of the LCL filter to shift towards lower frequencies, thus reducing the quality of the grid-connected current and affecting the power grid stability. To solve this problem, a hybrid active damping strategy with feedforward compensation is proposed for the neutral point clamped (NPC) LCL grid-connected inverter system. In order to reshape the output conductance of the grid-connected system, suppress the resonance spikes of the LCL filter and improve the adaptability of the grid-connected system to the weak grid. A first-order low-pass filter is designed in the grid-connected current loop, and an active damping control of grid-connected current based on a first-order high-pass filter is also proposed. Compared with the conventional capacitive current active damping, no additional sensors are required, and the use of a differential is avoided, which reduces the high-frequency noise. The use of passive resistors is reduced, which reduces the power loss of the grid-connected system. In addition, a point of common coupling (PCC) voltage feedforward strategy based on a low-pass filter is designed to suppress the background higher harmonics at PCC and improve the quality of grid-connected current. In this work, the robustness of the system is analyzed when the parameters of the LCL filter change. Finally, the virtual space vector modulation strategy is used to balance the neutral voltage of the DC bus. Simulation and experimental results show that the control strategy can effectively improve the adaptability of the system to the weak power grid, improve the quality of grid-connected current, and demonstrate strong stability. The THD can be decreased by 0.2% at least, and the improvements are more significant with larger line impedance; the THD is only 2.33% even at 10 mH line impedance.

Keywords: grid-connected inverter; weak grid; neutral point clamped (NPC); active damping; LCL filter; robustness

1. Introduction

Considering the non-renewable nature of traditional fossil fuels, it is imperative to develop energy systems in the direction of renewable energy [1]. With the proportion of renewable energy generation rapidly increasing, its grid-connected mode has changed from local grid-connected to centralized and distributed in multiple regions; the intermittent output of renewable energy begins to have an impact on the overall operation of the power grid, the stability problem between units and units, and between units and the power grid is more complicated [2]. Grid-connected inverters play a crucial role as interfaces between new energy generation systems and the grid [3]. However, the distributed power generation systems being scattered across various locations, coupled with long-distance transmission lines and a large number of transformer units, result in the grid-connected system exhibiting the characteristics of a weak grid with a low short circuit ratio [4]. The stability of the grid-connected inverter is heavily affected by the grid impedance under the weak grid condition [5].

The inverter circuit can only produce step waves directly, which requires filtering to integrate into the grid. The capacitance of the LC filter is directly connected in parallel at both ends of the grid voltage, which is equivalent to a capacitive load, which increases the difficulty of control. Compared with the L-type filter, the LCL filter has a lower cost and better high-frequency attenuation [6–9]. However, the LCL filter is a third-order underdamped system, which has a resonant peak at the resonant frequency. Additionally, the impedance of the power grid under weak grid conditions affects the frequency characteristics of the LCL filter, compromising the system's stability [10,11]. Typically, resonance suppression strategies for LCL filters include passive damping and active damping [12–14]. Although passive damping can effectively suppress the resonant peak of LCL, it increases the number of passive components, resulting in increased power consumption and introducing additional factors of system instability [15]. Therefore, active damping is usually preferred to suppress the resonant peak [16–18].

Literature [19] utilizes the filter capacitor current as the state variable and develops an active damping method to expand the effective damping area to improve grid stability. However, this method requires additional current sensors. Literature [20] proposed a capacitive current proportional feedback active damping, which effectively suppresses LCL resonance but does not consider weak grid conditions. Literature [21] proposed a capacitive current proportional feedback active damping with phase compensation, which has a good effect on the small range change of grid impedance. One study [22] uses the grid-connected current as the feedback variable and active damping in the form of differentiation to enhance the grid-connection effect. Nevertheless, this may amplify high-frequency noise, and the approximation error in the differential link implementation weakens the damping effect to some degree. Another study [23] incorporates a high-pass filter (HPF) in the grid-connected current feedback loop to construct a virtual impedance in parallel with the grid inductance to suppress the resonant peak, but it does not explore the grid connection control effect under weak grid conditions. Another study [24] proposes a hybrid damping control strategy that reduces the use of sensors and enhances the system's adaptability to weak grids. However, the use of passive devices increases the system's power loss.

In view of the existence of resonant spikes in the LCL filter, the grid impedance will affect the resonant frequency of the LCL, which leads to the instability of the grid-connected system, especially in the weak grid. Considering the inherent neutral point potential balance problem of the NPC inverter, a hybrid active damping strategy is proposed to improve the adaptability of the LCL converter in a weak grid. This work has the following features:

(1) Compared with the capacitive current active damping, the additional current sensor is eliminated, and the factors that may affect the system instability are reduced.
(2) Active damping of grid-connected current based on first-order HPF is adopted, and the use of the difference term is avoided, thus avoiding the error and high-frequency noise caused by the difference term.
(3) By avoiding the use of passive resistance, the adaptability of the grid-connected system to the weak grid is further improved, the quality of the grid-connected current is improved, and the system has high robustness.

The paper is structured as follows: Section 2 presents a discussion of the mathematical model and the original control strategy of the NPC grid-connected inverter system. Section 3 proposes an improved active damping control strategy. Section 4 discusses the neutral point potential balance strategy. Section 5 gives the simulation and experimental results. Section 6 summarizes the work.

2. System Mathematical Model and Stability Analysis

The NPC three-level inverter has been widely applied in the field of renewable energy, such as in solar power generation, wind power generation, and micro grid systems, due to its advantages of reducing harmonic content, improving energy conversion efficiency, high power application capability, reducing voltage stress, and strong adaptability. It

enables efficient conversion and integration of renewable energy, promoting the utilization of renewable energy and the sustainable development of power systems.

2.1. Mathematical Model of Three-Phase NPC LCL Grid-Connected Inverter

The main circuit of a three-phase, NPC-type LCL grid-connected inverter is illustrated in Figure 1. The inverter features two clamping diodes and four IGBTs per bridge arm. The DC-side voltage-dividing capacitors, C_1 and C_2, are connected to point O at the midpoint of the clamping diodes, halving the DC-side voltage U_{dc} of each IGBT when it is switched off. The LCL filter comprises the inductance L_1, the filter capacitor C, and the grid-side inductance L_2. The inverter output current is denoted by i_{1x} (x = a, b, c), the grid-connected current is represented by i_{2x}, the capacitor current is expressed as i_{Cx}, the inverter output voltage is indicated by U_x, the capacitor voltage is denoted by U_{cx}, and the grid voltage is represented by U_{gx}. Typically, the grid impedance comprises both resistive and inductive components. This paper focuses on analyzing the stability of the grid-connected system by considering solely the presence of an inductive component, L_g, as the inclusion of a resistive component is known to contribute to the system's stability.
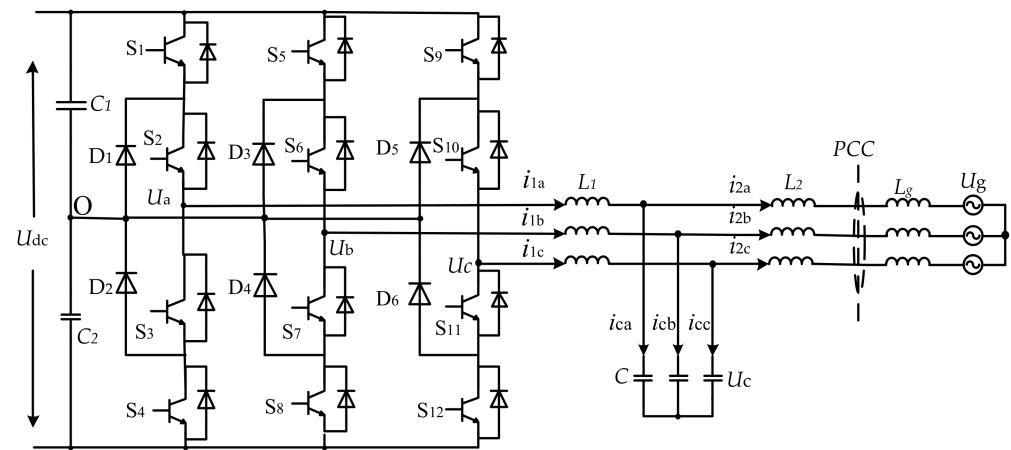

Figure 1. Three-phase NPC LCL grid-connected inverter topology structure.

The mathematical model for three-phase, NPC-type LCL grid-connected inverter can be represented as Equation (1) in a three-phase stationary coordinate system.

$$\begin{cases} U_x = U_{cx} + L_1 \frac{di_1}{dt} \\ U_{cx} = U_{gx} + (L_2 + L_g) \frac{di_2}{dt} \\ i_{1x} = i_{2x} + C \frac{dU_{cx}}{dt} \end{cases} \tag{1}$$

The mathematical model in the s-domain of a two-phase stationary coordinate system can be obtained by applying the Clarke transformation and Laplace transformation to Equation (1), as depicted in Equation (2).

$$\begin{cases} U_{\alpha\beta}(s) = U_{C\_\alpha\beta}(s) + sL_1 i_{1\_\alpha\beta}(s) \\ U_{C\_\alpha\beta}(s) = U_{g\_\alpha\beta}(s) + s(L_2 + L_g) i_{2\_\alpha\beta}(s) \\ i_{1\_\alpha\beta}(s) = i_{2\_\alpha\beta}(s) + sCU_{c\_\alpha\beta}(s) \end{cases} \tag{2}$$

2.2. System Stability Analysis

To facilitate analysis and research, the three-phase grid-connected inverter is transformed from the d q coordinate system to the $\alpha\beta$ stationary coordinate system. This transformation is necessary due to the coupling inherent in the former. Based on Figure 1 and Equation (2), the control block diagram in the α coordinate axis of the inverter can be obtained, as shown in Figure 2, taking the α coordinate axis as an example.
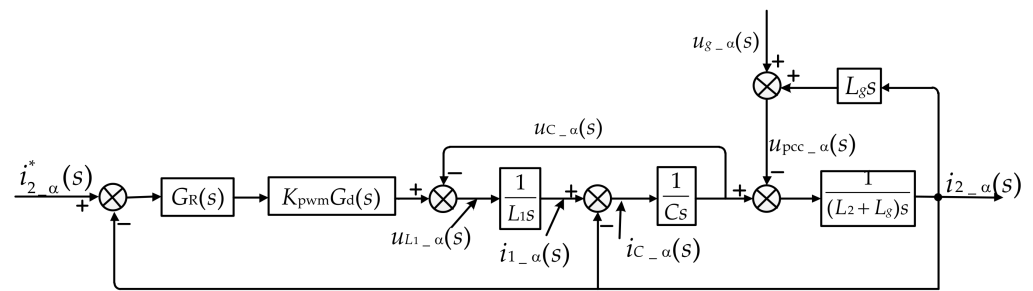
Figure 2. Control diagram of the grid-connected inverter (α).

As shown in Figure 2, $i^*_{2\_\alpha}(s)$ represents the given reference current; $u_{g\_\alpha}(s)$ represents the grid-connected voltage of α-axis; $u_{pcc\_\alpha}(s)$ is the common coupling point voltage of the α-axis; $u_{c\_\alpha}(s)$ denotes the filter capacitor voltage of the α-axis; K_{pwm} is the modulation gain of the inverter, which is U_{dc}/U_{tri}, where U_{tri} is the amplitude of the triangular carrier wave; $G_d(s)$ represents the delay caused by digital computation and modulation signals, which is typically 1.5 sampling periods and can be expressed as Equation (3), and perform Padè approximation; $G_R(s)$ is the quasi-proportional resonance (QPR) controller for current loop quasi-proportional tracking in the $\alpha\beta$ coordinate system, the QPR controller has better tracking performance compared to the PI controller. It has a higher gain at the fundamental frequency and provides some suppression effect on high-frequency harmonics. Its transfer function is given by Equation (4).

$$G_d(s) = e^{-1.5Ts} \approx \frac{1 - 0.75T_s s}{1 + 0.75T_s s} \qquad (3)$$

$$G_R(s) = K_p + \frac{2K_r\omega_c s}{s^2 + 2\omega_c s + \omega_0^2} \qquad (4)$$

where, K_p is the proportional coefficient of $G_R(s)$; K_r is the resonant coefficient; ω_0 is the fundamental angular frequency, where $\omega_0 = 2\pi f_0$ and f_0 is the fundamental frequency; ω_c is the cut-off bandwidth of the QPR controller; T_s is the sampling period.

In order to solve the instability of the grid-connected system caused by grid impedance. Scholars are more inclined to adopt active damping control than passive damping control. In some articles, the phase margin of the system is improved by adding a phase compensation link to the control loop of the grid-connected inverter. However, most of the phase compensation links are advanced links, which will amplify the high-frequency harmonics in the loop. In some articles, suppressing resonance based on adaptive filtering is proposed, but the algorithm process is cumbersome and is not conducive to practical engineering applications. The active damping control based on the filter suppresses the resonance, obviously, and the process is simple and easy to implement.

In reference [24], a hybrid damping control strategy that integrates active damping and passive damping was proposed. The grid current control loops the addition of a low-pass filter (LPF), with the voltage at the common coupling point utilized as voltage feedforward through the LPF. Furthermore, a passive damping resistor R is connected in series with the filter capacitor. The control block diagram of the system is depicted in Figure 3.

In Figure 3, $G_f(s)$ and $G_s(s)$ are first-order LPF, and the filtering effect is achieved by reducing the amplitude of high-frequency signals. Properly designing the parameters enables the smoothing of the input signal and the removal of high-frequency noise, and their transfer functions are given by Equation (5). The open-loop transfer function of the system is given by Equation (6).

$$G_f(s) = G_s(s) = \frac{1}{n_{1s} + 1} \qquad (5)$$

$$G_o(s) = \frac{i_{2\_\alpha}(s)}{i*_{2\_\alpha}(s)} = \frac{(RC_s + 1)K_{pwm}G_R(s)G_d(s)}{B_1 s^3 + (B_2 - B_3)(RCs^2 + s)} \tag{6}$$

where, n_1 is the tuning parameter, and a value of $n_1 = 4 \times 10^{-5}$ is used in the paper. $B_1 = L_1(L_2 + L_g)$ C, $B_2 = L_1 + L_2 + L_g$, and $B_3 = L_g G_f(s)G_d(s)$.

According to Equation (5), in order to verify the stability of the system under different grid-side line impedances, the open-loop frequency response Bode diagram of the system is plotted, as shown in Figure 4. It can be seen from the figure that as the grid line impedance gradually increases, the phase margin (PM) of the system decreases while the gain margin (GM) changes less. When $L_g = 9$ mH, the system phase margin is only 19.4°, which does not meet the engineering application requirements. In addition, the passive component R increases the power loss in the system, so optimization of this control strategy is necessary.
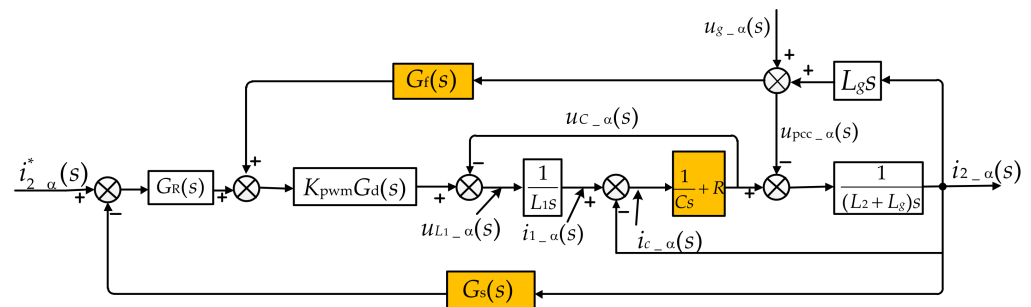

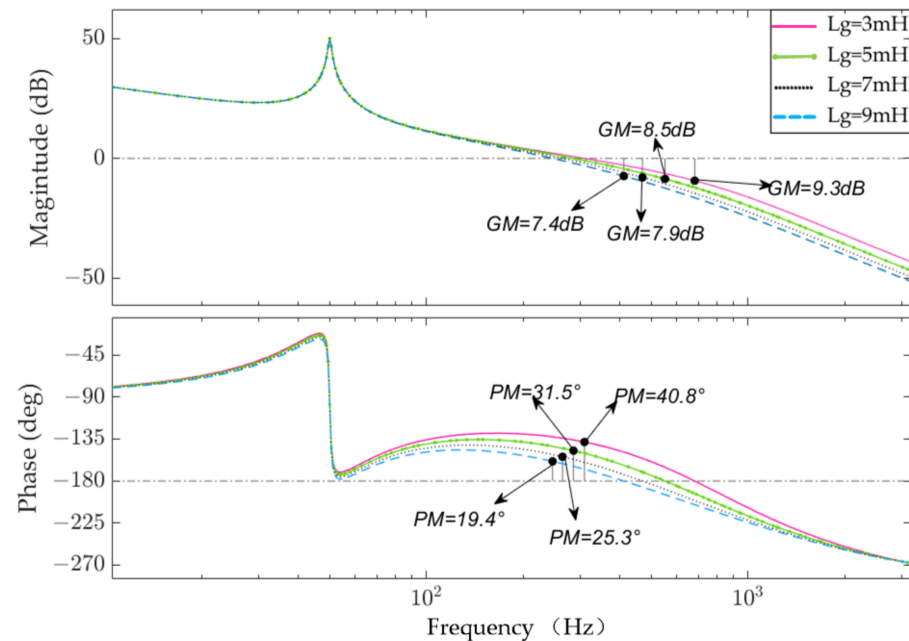**Figure 3.** Control diagram of the hybrid damping system (α).

Figure 4. Open-loop Bode diagram of the hybrid damping system.

3. Hybrid Active Damping Control Strategy with Feedforward Compensation

The active capacitor current damping method is commonly used to suppress the LCL resonance peak. However, to avoid the additional use of current sensors, a grid current active damping method is proposed. Figure 5 illustrates the system block diagram of the active grid current damping method, where the proportional feedback factor is represented by K_{AD}.
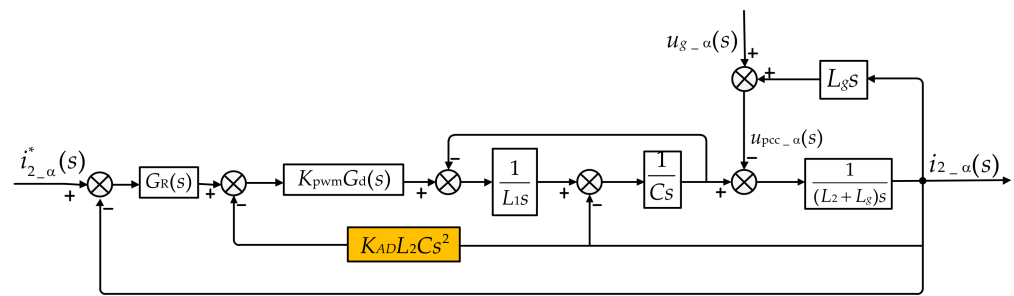
Figure 5. Diagram of grid-connected current active damping (α).

Differentiation will amplify high-frequency noise in practical applications, which is not conducive to grid-connected control, and achieving the ideal differentiation is also difficult. Additionally, the approximation error weakens the damping effect. To enhance system stability margin and adaptability to weak grids, a hybrid active damping control strategy with feedforward compensation is proposed in this paper to address the issues associated with differentiation. A first-order LPF is incorporated into the current loop to reshape the output admittance and enhance the system stability margin. Active damping based on the first-order HPF feedback of the grid current replaces the differentiation variable in the active grid current damping method to suppress the resonance peak of the LCL filter. Furthermore, the voltage at the common coupling point is utilized as feedforward compensation through a first-order LPF to improve the grid-connected current quality of the system. Figure 6 illustrates the system structure further.
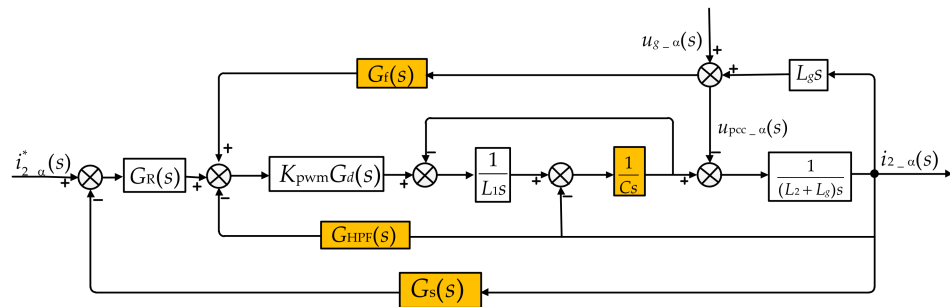

Figure 6. Diagram of hybrid active damping system with feedforward compensation (α).

In Figure 6, $G_{\mathrm{HPF}}(s)$ is a first-order HPF; by properly designing the parameters, high-frequency components can be extracted to construct the damping component with a transfer function given by Equation (7). The open-loop transfer function of the system is given by Equation (8). It can be seen that it is a fourth-order model, which has a better suppression effect on high-frequency components.

$$G_{\mathrm{HPF}}(s) = \frac{K_{\mathrm{h}}s}{s + \omega_{\mathrm{h}}} \tag{7}$$

$$G'_o(s) = \frac{K_{\mathrm{pwm}}G_{\mathrm{R}}(s)G_{\mathrm{d}}(s)(s + \omega_{\mathrm{h}})}{A_1(s^4 + \omega_{\mathrm{h}}s^3) + (B_2 - B_3)(s^2 + \omega_{\mathrm{h}}s) + A_2 s} \tag{8}$$

In the equations, $A_1 = L_1(L_2 + L_g)C$, $A_2 = K_{\mathrm{h}}G_{\mathrm{d}}(s)$, $B_2 = L_1 + L_2 + L_g$, and $B_3 = L_gG_{\mathrm{f}}(s)G_{\mathrm{d}}(s)$; K_{h} and ω_{h} are the parameters of the HPF, and their relationship must satisfy Equation (9).

$$\begin{cases} K_{\mathrm{h}} = \omega_{\mathrm{ref}}(L_1 + L_2)(2 - k_2)\sqrt{1 - k^2} \\ \omega_{\mathrm{h}} = 2\omega_{\mathrm{ref}}\sqrt{1 - k^2} \end{cases} \tag{9}$$

The value of *k* ranges from 0.8 to 0.9, and a value of *k* = 0.85 is used. ω_{ref} is the open-loop resonant angular frequency, which can be obtained from Equation (10):

$$\omega_{\text{ref}} = 2\pi f_{\text{ref}} = \sqrt{\frac{L_1 + L_2 + L_g}{L_1(L_2 + L_g)C}} \tag{10}$$

Combining Equations (9) and (10), we can obtain $K_h = 7$ and $\omega_h = 3500$.

To evaluate the effectiveness of the proposed control strategy, the open-loop frequency response of the system is analyzed under different grid line impedances. As demonstrated in Figure 7, the system's phase margin improves to varying degrees after implementing the proposed strategy. Even with a grid-side line impedance of 9 mH, the system gain margin is 8.7 dB, and the phase margin is 35.1°, meeting the requirements of system stability and engineering applications. In comparison to the hybrid damping strategy, the proposed approach notably enhances the system's phase margin and stability.
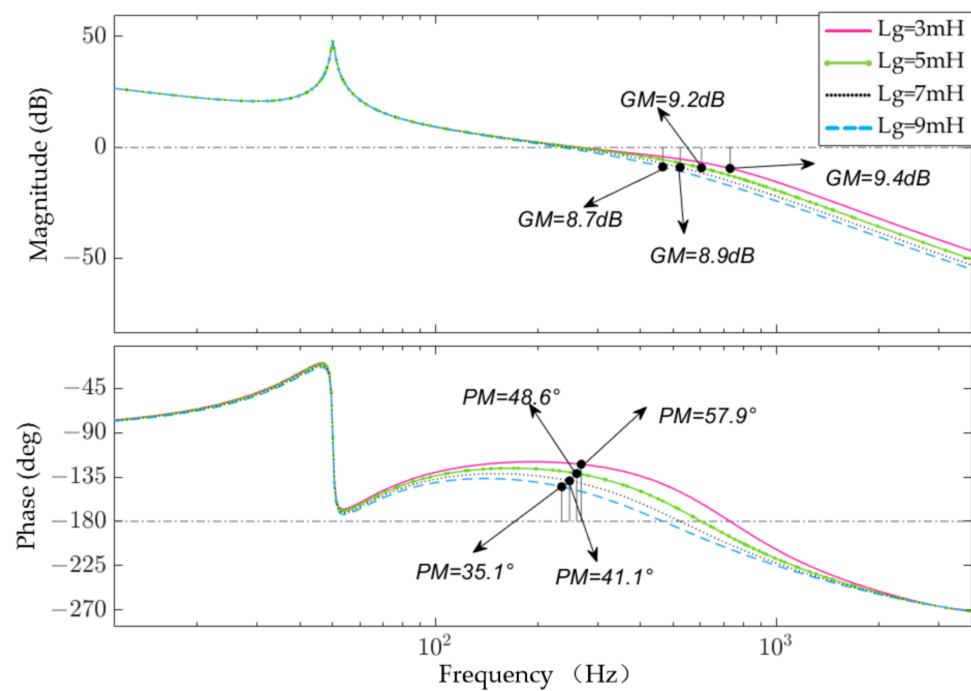

Figure 7. Open-loop Bode plot of hybrid active damping system with feedforward compensation.

In practical operation, LCL filter parameters may change. To verify the system's robustness under LCL parameter variations, open-loop Bode diagrams of the system are plotted for different LCL filter parameter variations under a grid line impedance with poor grid connection conditions (L_g = 9 mH), as illustrated in Figure 8.

Figure 8 reveals that the system's stability can be maintained even when the parameters of the LCL filter components change, and both the phase margin and gain margin have good margins. These results demonstrate that the proposed hybrid active damping system with feedforward compensation exhibits robust stability.
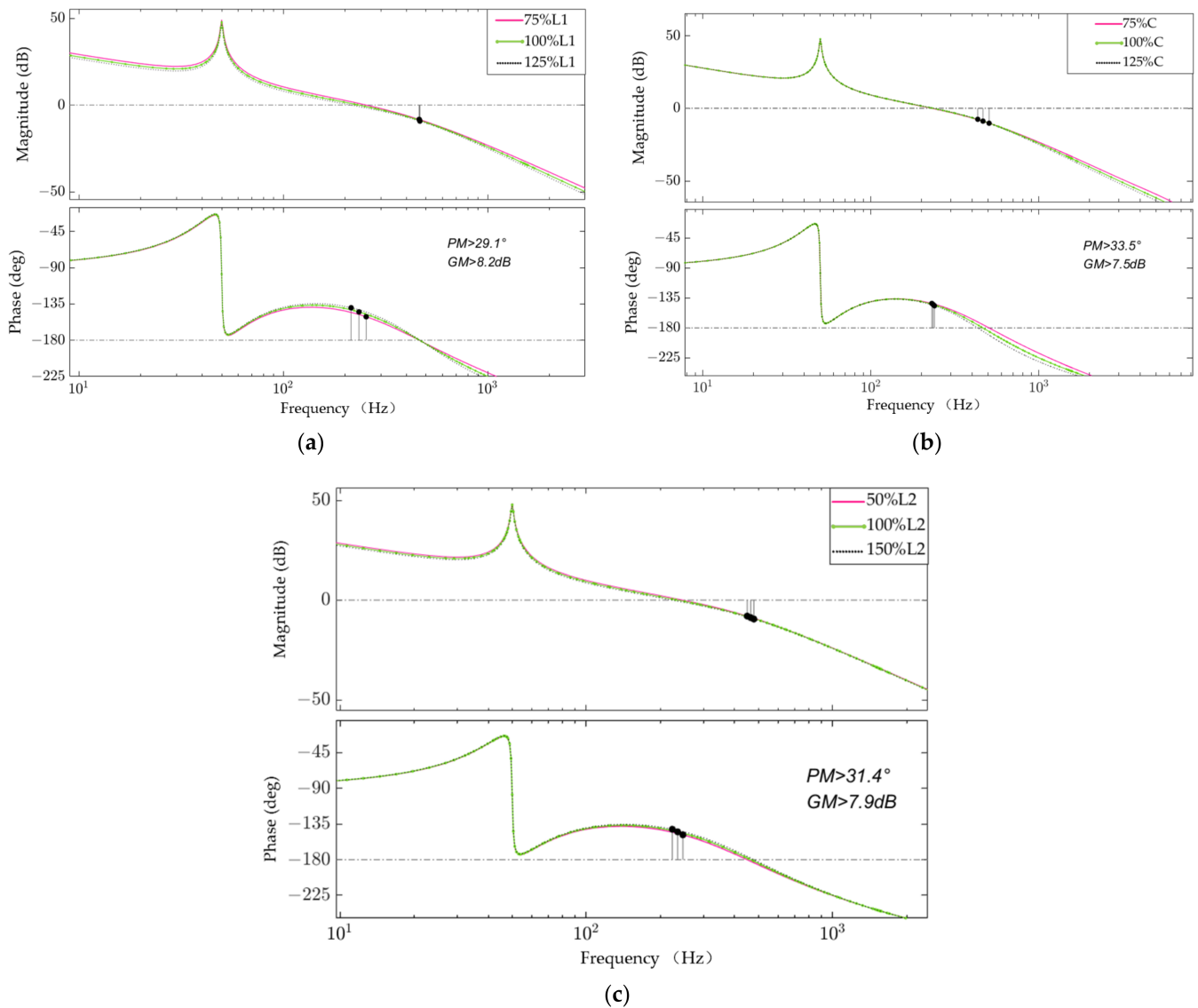
(a)

(b)

(c)

Figure 8. Open-loop Bode diagram of systems with changing filter parameters. (**a**) Bode diagrams of the system when the inverter-side inductance varies; (**b**) Bode diagrams of the system when the filter capacitor varies; (**c**) Bode diagrams of the system when the grid-side inductance varies.

4. Neutral-Point Potential Balancing Strategy

In order to test the grid-connected control effect of the hybrid active damping strategy with feedforward compensation under weak grid conditions, a grid-connected controller is designed. However, the fluctuation of DC-side neutral-point potential is an inherent issue in NPC inverters, and a deviation in the neutral-point potential can increase the switch stress and decrease the lifespan of power devices. Furthermore, it can elevate high-order harmonics in the inverter's output voltage, which can affect the quality of the grid-connected current. To mitigate this problem, the virtual space vector pulse width modulation (VSVPWM) technique is utilized in this study for the purpose of controlling the neutral-point potential.

Figure 9 illustrates the classification of vectors into 3 zero vectors, 12 small vectors, 6 medium vectors, and 6 large vectors based on their length. The zero vectors (PPP, NNN, OOO) and large vectors (PNN, PPN, NPN, NPP, NNP, PNN) do not affect the neutral-point potential, while the medium and small vectors can produce fluctuations in the neutral-point potential. Table 1 shows the midpoint current generated by the medium and small vectors.
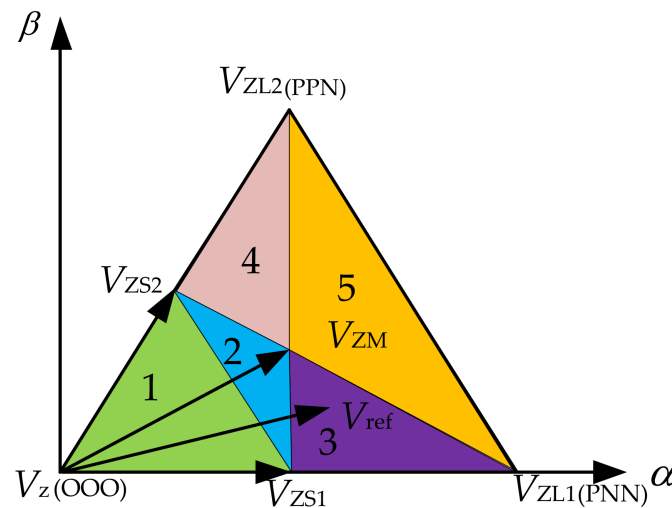
Table 1. The relationship between the voltage vector and the neutral-point current

Classification of Vectors	Vector	Neutral-Point Current
Medium Vector	OPN	i_a
	PON	i_b
	NPO	i_c
	ONP	i_a
	NOP	i_b
	PNO	i_c
Positive Small Vector	OPP	i_a
	POP	i_b
	NNO	i_c
	ONN	i_a
	NON	i_b
	PPO	i_c
Negative Small Vector	POO	$-i_a$
	OPO	$-i_b$
	OON	$-i_c$
	NOO	$-i_a$
	ONO	$-i_b$
	OOP	$-i_c$

Figure 9. Space voltage vector diagram of three-level inverter.

The virtual space vector pulse width modulation (VSVPWM) technique creates a virtual vector by combining small and medium vectors, which ensures that the average current flowing into and out of the DC bus midpoint is zero within one control cycle, thereby balancing the neutral-point potential. Figure 10 depicts the distribution of virtual space vectors for VSVPWM in the Sector I, which can be divided into five sub-sectors represented by 1, 2, 3, 4, and 5 respectively, and Equation (11) represents the synthesis rule. The synthesis rules for the other sectors are identical.

$$\begin{cases} V_Z = V_{O(OOO)} \\ V_{ZS1} = \frac{1}{2}\left(V_{S1(ONN)} + V_{S1(POO)}\right) \\ V_{ZS2} = \frac{1}{2}\left(V_{S2(PPO)} + V_{S2(OON)}\right) \\ V_{ZM} = \frac{1}{3}\left(V_{S1(ONN)} + V_{M(PON)} + V_{S2(PPO)}\right) \\ V_{ZL1} = V_{L1(PNN)} \\ V_{ZL2} = V_{L2(PPN)} \end{cases} \qquad (11)$$

Figure 10. Space voltage vector diagram of VSVPWM.

VSVPWM technique utilizes virtual vectors that are synthesized from the combinations of small and medium vectors to achieve neutral-point potential balancing. In this context, $V_{O(OOO)}$ is a basic zero vector, $V_{S1(ONN)}$, $V_{S1(POO)}$, $V_{S2(PPO)}$, and $V_{S2(OON)}$ are two pairs of redundant basic small vectors, $V_{M(PON)}$ represent a basic middle vector, $V_{L1(PNN)}$ and $V_{L2(PPN)}$ represent a basic large vector. V_Z denotes the virtual zero vector, V_{ZS1} and V_{ZS2} represent the virtual small vectors, V_{ZM} denotes the virtual medium vector, and V_{ZL1} and V_{ZL2} represent the virtual large vectors. Specifically, the virtual small vector is composed of two pairs of redundant basic small vectors. By controlling the action time of the two redundant vectors, the average current flowing into the midpoint potential of the bus is 0, which avoids the influence on the midpoint potential. The action time of the three space voltage vectors in the virtual is the same. Due to the three-phase three-wire structure, the current flowing into the midpoint potential of the bus is $i_a + i_b + i_c = 0$ to avoid the midpoint potential fluctuation; the action of the virtual large vector will not affect the midpoint potential; VSVPWM achieves the balance of the midpoint potential by controlling that the average value of the midpoint potential current of the inflow and outflow bus bar in each modulation period is zero.

5. Simulation and Experimental Results Analysis

5.1. Analysis of Simulation Results

To confirm the accuracy of the theoretical analysis mentioned earlier and evaluate the efficacy of the proposed control strategy, a system model was constructed in MATLAB/Simulink (2021a), as depicted in Figure 11. The system parameters can be found in Table 2.

Table 2. System parameters.

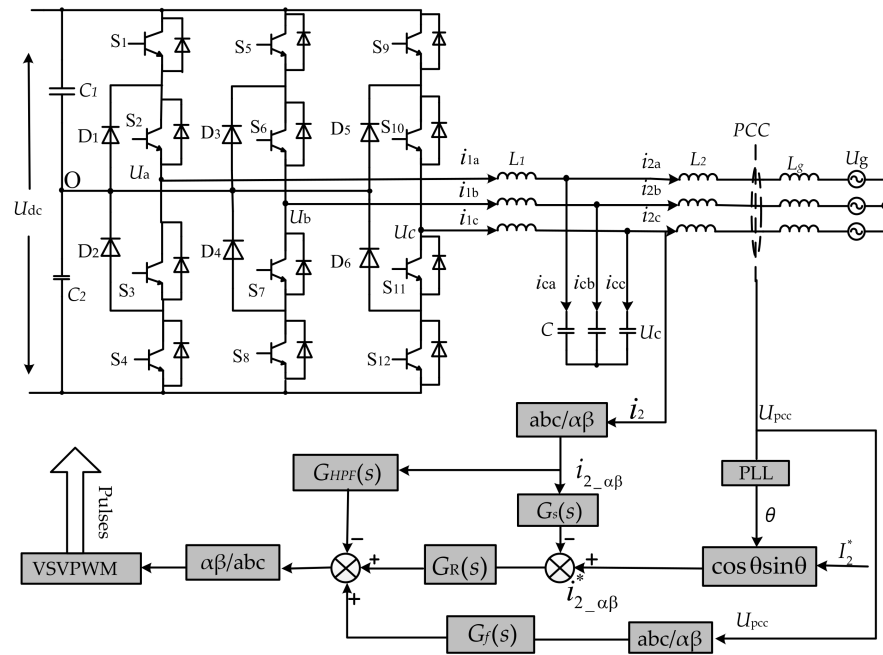| Parameter	Numerical Value
DC bus voltage, U_{dc}	350 V
Voltage divider capacitor, C_1, C_2	680 μF
Inverter side inductance, L_1	2.4 mH
Filter capacitor, C	10 μF
Net side electrical feeling, L_2	0.6 mH
Proportionality factor, K_p	12
Resonance factor, K_r	700
Cutoff bandwidth, ω_c	3.14
Frequency of sampling, f_s	10 kHz

Figure 11. LCL grid-connected inverter with feedforward compensation hybrid active damping.

Figure 12 shows the grid current waveform when the system is in a stable state during L_g = 4.2 mH. After adopting the hybrid damping control strategy proposed in reference [24], the total harmonic distortion (THD) of grid-connected current is 1.23%, which improves the quality of grid-connected current under a weak power grid. In addition, by adding the damper control strategy proposed in this paper, the THD of grid-connected current is further reduced to 1.03%. Because the impedance of the network side is not very high, the characteristics of the weak network are not strong enough. The two damping strategies proposed in reference [24] and in this study ensure the stable operation of the grid-connected system, and the vibration reduction strategy proposed in this paper slightly improves the quality of the grid-connected current.

To further verify the effectiveness of this strategy in a weak grid, Figure 13 shows the grid current waveforms of the system when the grid impedance L_g increases to 8 mH. With the increase in grid impedance, the hybrid damping strategy proposed in reference [24] can stabilize the grid-connected system. However, this stability comes at the expense of reducing the current quality of the grid, with a total harmonic distortion (THD) of 2.67%. On the contrary, the feedforward compensation hybrid active damper proposed in this paper maintains a low THD level (1.33%) and reduces THD by 1.34%, which effectively improves the quality of grid current.

With the increase in the grid impedance (L_g = 10 mH), The harmonic of the grid current increases in the hybrid vibration control system of Reference [24], and the quality of the grid-connected current is seriously distorted, which leads to the unstable operation of the grid-connected system, as shown in Figure 14. However, the proposed damping control strategy can still have good grid-connected current quality, and the total harmonic distortion (THD) is only 2.33%, which can ensure the stability of the grid-connected system.

The simulation results show that the greater the grid impedance is, the worse the grid characteristics are, the worse the grid-connected condition of the inverter is, and the worse the current quality is. The coupling point voltage feedforward of grid-connected current and the control strategy of the hybrid active damper are adopted to make the system operate stably in different degrees of the weak grid while maintaining a good sinusoidal waveform. With the increase in the line impedance, the total harmonic distortion rate of grid-connected current can still be kept at a low level. Therefore, the proposed control strategy can effectively enhance the stability and adaptability of the system to weak grid scenarios.
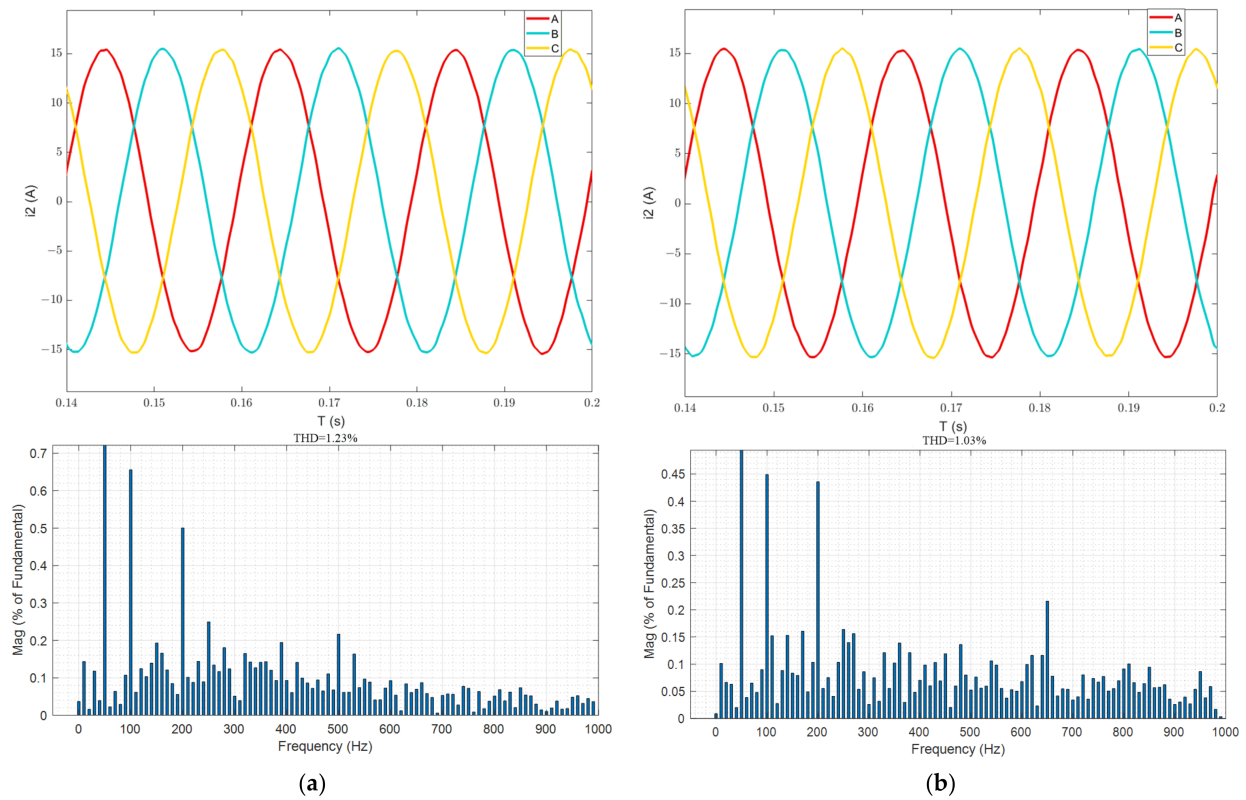
Figure 12. Steady-state grid-connected current waveform (L_g = 4.2 mH). (**a**) Hybrid damping; (**b**) Hybrid active damping with feedforward compensation.
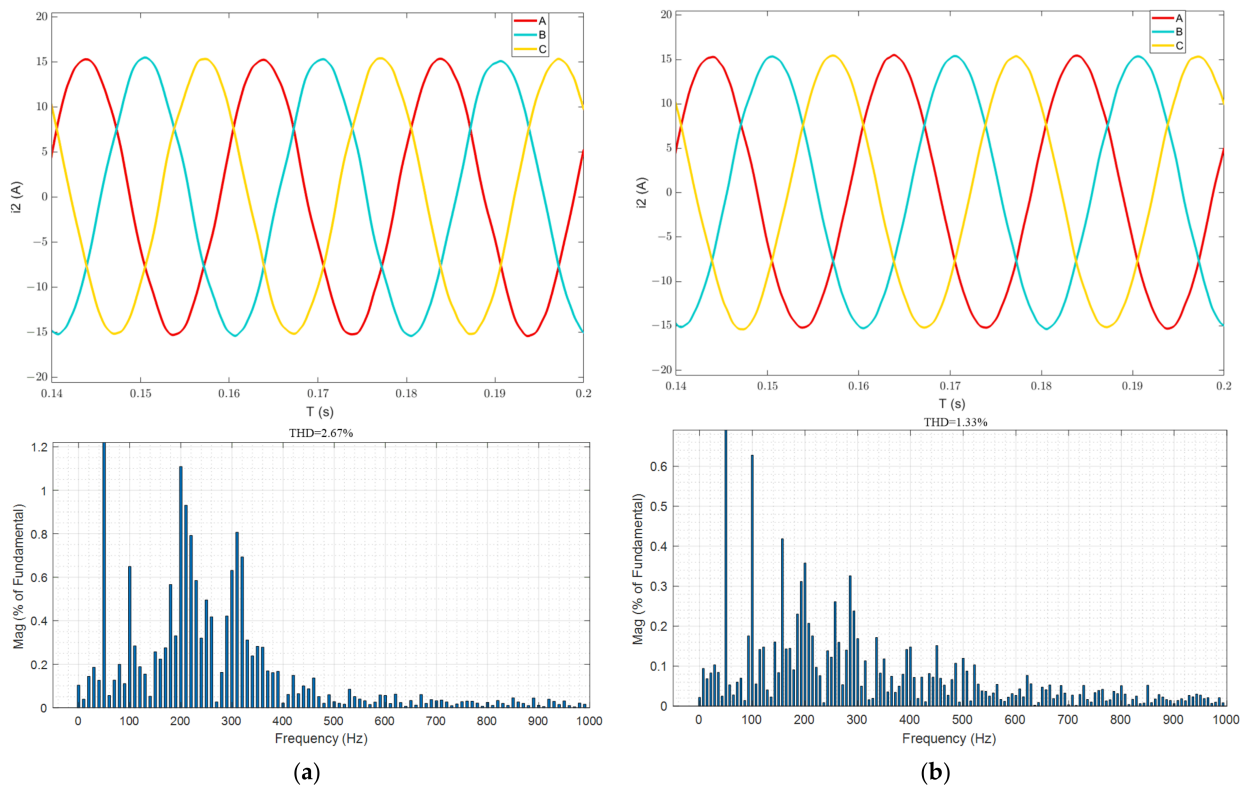

Figure 13. Steady-state grid-connected current waveform (L_g = 8 mH). (**a**) Hybrid damping; (**b**) Hybrid active damping with feedforward compensation.
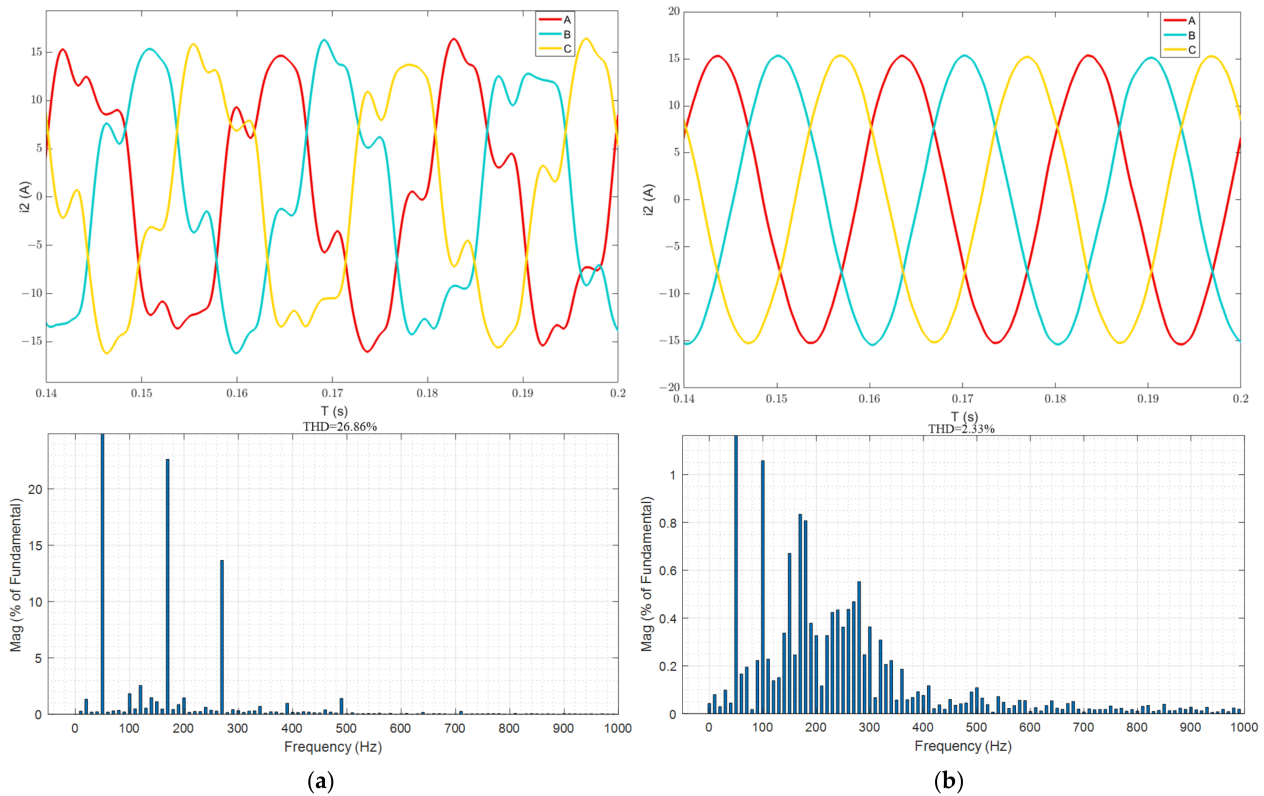
Figure 14. Steady-state grid-connected current waveform (L_g = 10 mH). (**a**) Hybrid damping; (**b**) Hybrid active damping with feedforward compensation.

5.2. Analysis of Experimental Results

In order to validate the accuracy and efficacy of the proposed control strategy in this paper, a three-phase bridge grid-tied inverter experimental platform that corresponds to the proposed strategy was constructed in the laboratory. The experimental parameters are consistent with the simulation parameters. The back-stage LCL filter of the test bed is connected to the power grid through auto-transformer, isolation-transformer, and line impedance (L_g). The ratio of the auto-transformer is 380 to 150. The complete experimental prototype is depicted in Figure 15.
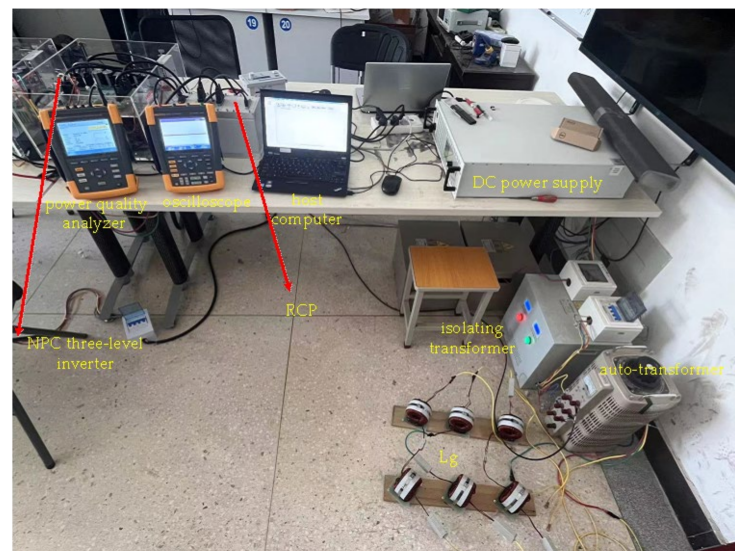
Figure 15. Experimental prototype.

The experimental setup comprises a programmable DC power supply from German EA company (EA-PSI 9500-60, Viersen, Germany), an NPC three-level inverter (YXPHM-TP310b-I) produced by Nanjing Yanxu Electric Co. Ltd. in Nanjing, China with signal detection and drive systems, an LCL filter, a grid-connected transformer, a rapid controller prototyping (RCP) of YXSPACE-10 produced by Nanjing Yanxu Electric Co. Ltd. in China, and a host computer. Prominent testing instruments include a Fluke 190-204S oscilloscope and a Fluke 435 II power quality analyzer produced by Fluke Corporation in Everett, WA, USA. Simulation analysis is carried out by constructing system models and controllers in the MATLAB/Simulink (2021a) environment on the host computer. The real-time control of the inverter is achieved using the RCP prototype controller, based on the results of the simulation analysis, to verify the practical effectiveness of the proposed algorithm. In order to simulate the grid impedance (L_g), a specific value of inductance is connected in series on the grid side.

The comparison between Figures 16 and 17 shows that the experimental waveform confirms the effectiveness of the proposed control strategy. Figure 16 shows that in the absence of grid impedance, the two control strategies show stable operation and low harmonics, indicating that they meet the requirements of grid connection under the condition of a strong power grid. Figure 17a shows that when L_g = 4.2 mH and the hybrid damping strategy of Ref. [24] are adopted, the harmonic component of the grid current increases. However, the improved control strategy, as shown in Figure 17b, effectively reduces the harmonic component by 1.1% compared with the previous control system. The improved control strategy significantly improves the current quality of the power grid, thus expanding the scope of application of the weak power grid, enhancing the stability of the system, and improving the ability to suppress harmonics.
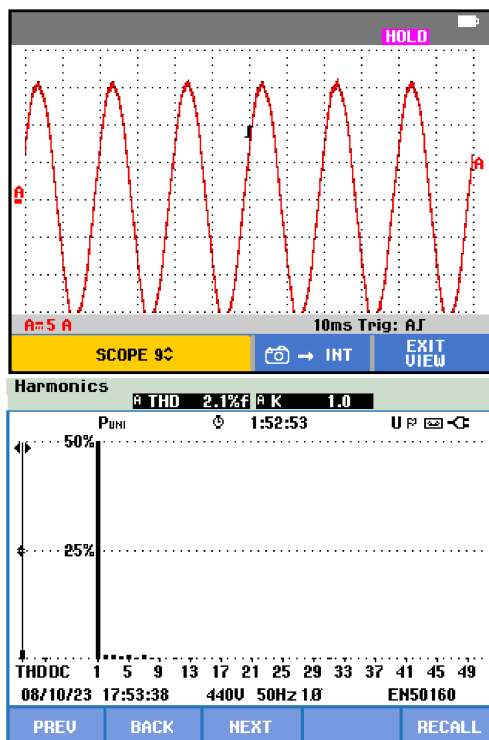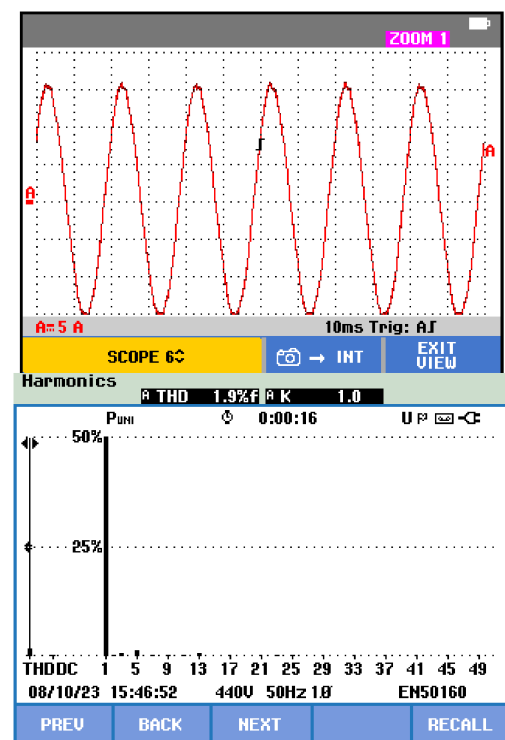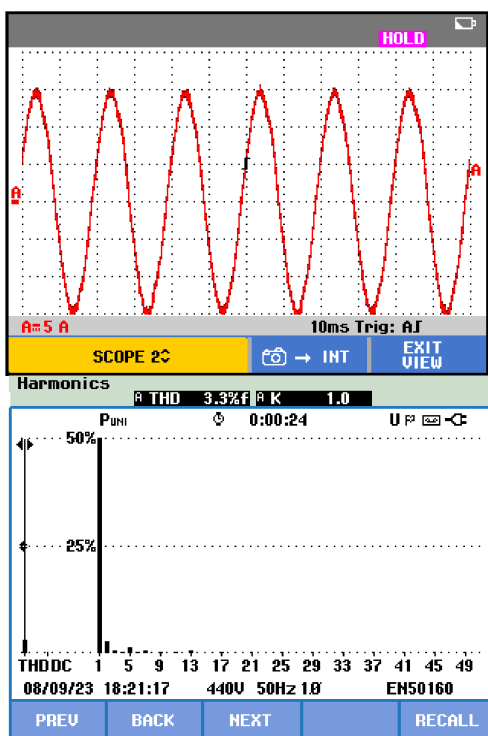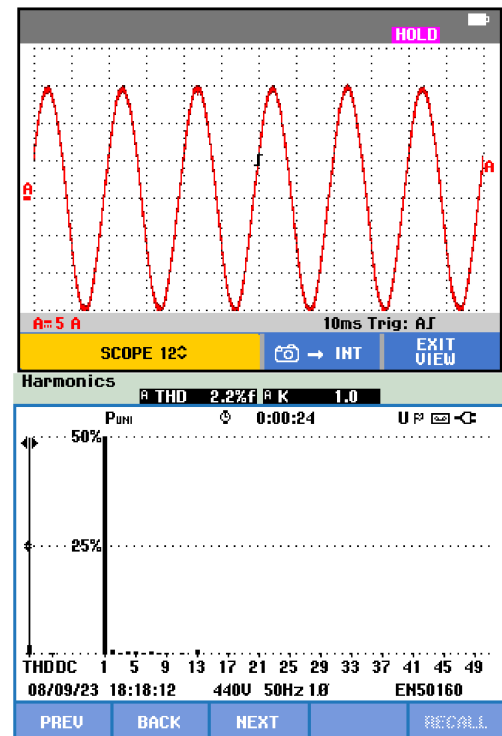

(**a**)   (**b**)

Figure 16. Experimental results of two strategies (L_g = 0 mH). (**a**) Hybrid damping; (**b**) Hybrid active damping with feedforward compensation.

Figure 17. Experimental results of two strategies (L_g = 4.2 mH). (**a**) Hybrid damping; (**b**) Hybrid active damping with feedforward compensation.

6. Conclusions

In order to solve the problem of resonant frequency deviation caused by grid impedance in an LCL grid-connected inverter system under the condition of a weak power grid, reduce the robustness of the system, and affect the stability of the grid connection, a hybrid active damping strategy with feedforward compensation is proposed. We design a hybrid active damping strategy with grid-connected current as a state variable to suppress the resonant peak of the LCL filter. Compared with the traditional capacitive current active damping method, this method does not need additional current sensors. In order to further improve the stability margin of the system and improve the adaptability of the system to the grid impedance (PM relative increase of about 15°), a first-order LPF is designed in the current loop, and a coupling point voltage feedforward strategy through HPF is adopted. Compared with the hybrid damping control strategy, this control strategy reduces the use of passive resistors, thus reducing the power loss of the system. In addition, under the control strategy of this paper, good current quality can be maintained even under the larger grid impedance. Simulation and experimental results verify the effectiveness of the control strategy and improve the current quality of the power grid; when the grid impedance is low, the current exhibits a favorable total harmonic distortion (THD) level of less than 1.5%. Even as the impedance increases, the current is still able to maintain a satisfactory THD level of less than 2.5%, which enhances the adaptability of the system within the weak power grid and has strong, robust stability (PM remained stable at about 30°). In future research, it is necessary to address the challenges posed by unbalanced power grids, as they can lead to significant detrimental effects. Future investigations should focus on studying unbalanced, weak power grids to mitigate their impact. Furthermore, the parameter identification module can be further integrated to enable real-time detection of grid impedance while dynamic adjustment of filter parameters to enhance grid-connected performance.

References

1. Wu, Q.H.; Bose, A.; Singh, C.; Chow, J.H.; Mu, G.; Sun, Y.Z.; Liu, Z.X.; Li, Z.G.; Liu, Y. Control and Stability of Large-scale Power System with Highly Distributed Renewable Energy Generation: Viewpoints from Six Aspects. *CSEE J. Power Energy Syst.* **2023**, *9*, 8–14.
2. Shah, H.; Chakravorty, J.; Chothani, N.G. Protection Challenges and Mitigation Techniques of Power Grid Integrated to Renewable Energy Sources: A Review. *Energy Sources Part A Recovery Util. Environ. Eff.* **2023**, *45*, 4195–4210. [CrossRef]
3. Blaabjerg, F.; Teodorescu, R.; Liserre, M.; Timbus, A.V. Overview of Control and Grid Synchronization for Distributed Power Generation Systems. *IEEE Trans. Ind. Electron.* **2006**, *53*, 1398–1409. [CrossRef]
4. Gupta, B.K.; Sekhar, K.R. A Current Controller Gain Characterization of Weak Grid Coupled Solar Inverter Through Impedance Interaction Modeling. *IEEE Trans. Ind. Electron.* **2023**, *7*, 2520–2530. [CrossRef]
5. Lin, Z.; Ruan, X.; Zhang, H.; Wu, L. A Generalized Real-time Computation Method with Dual-sampling Mode to Eliminate the Computation Delay in Digitally Controlled Inverters. *IEEE Trans. Power Electron.* **2022**, *37*, 5186–8195. [CrossRef]
6. Li, S.Q.; Zhou, S.S.; Li, H.P. Harmonic Suppression Strategy of LCL Grid-Connected PV Inverter Based on Adaptive QPR_PC Control. *Electronics* **2023**, *12*, 2282. [CrossRef]
7. Xu, J.M.; Xie, S.J. LCL-resonance Damping Strategies for Grid-connected Inverters with LCL Filters: A Comprehensive Review. *J. Mod. Power Syst. Clean Energy* **2018**, *6*, 292–305. [CrossRef]
8. Yang, L.; Yang, J.; Gao, M.; Watson, A.; Wheeler, P. Current Control of LCL-type Shunt APFs: Damping Characteristics, Stability Analysis, and Robust Design Against Grid Impedance Variation. *IEEE J. Emerg. Sel. Topics Power Electron.* **2021**, *9*, 5026–5042. [CrossRef]
9. Radwan, A.A.A.; Mohamed, Y.A.-R.-I. Grid-connected Wind-solar Cogeneration Using Back-to-back Voltage-source Converters. *IEEE Trans. Sustain. Energy* **2020**, *11*, 315–325. [CrossRef]
10. Li, X.; Lin, H. A Design Method of Phase-locked Loop for Grid-connected Converters Considering the Influence of Current Loops in Weak Grid. *IEEE J. Emerg. Sel. Topics Power Electron.* **2020**, *8*, 2420–2429. [CrossRef]
11. Zeng, C.B.; Wang, H.W.; Miao, H. Grid-Voltage-Feedback Active Damping with Lead Compensation for LCL-Type Inverter Connected to Weak Grid. *IEEE Access* **2021**, *9*, 106813–106823. [CrossRef]
12. Yang, Z.; Shah, C.; Chen, T.; Teichrib, J.; De Doncker, R.W. Virtual Damping Control Design of Three-phase Grid-tied PV Inverters for Passivity Enhancement. *IEEE Trans. Power Electron.* **2021**, *36*, 6251–6264. [CrossRef]
13. Huang, X.; Wang, K.; Fan, B.; Yang, Q.; Li, G.; Xie, D.; Crow, M.L. Robust Current Control of Grid-tied Inverters for Renewable Energy Integration under Non-Ideal Grid Conditions. *IEEE Trans. Sustain. Energy* **2020**, *11*, 477–488. [CrossRef]
14. Yang, L.; He, X.; Zhang, P.; Liu, S. Control Scheme and Performance Analysis of Dual-frequency Single-phase Grid-connected Inverter Interfaced with Weak and Distorted Grids. *IEEE Access* **2020**, *8*, 178639–178650. [CrossRef]
15. Peña-Alzola, R.; Liserre, M.; Blaabjerg, F.; Sebastián, R.; Dannehl, J.; Fuchs, F.W. Analysis of the Passive Damping Losses in LCL-Filter-Based Grid Converters. *IEEE Trans. Power Electron.* **2013**, *28*, 2642–2646. [CrossRef]
16. Rodriguez-Diaz, E.; Freijedo, F.D.; Vasquez, J.C.; Guerrero, J.M. Analysis and Comparison of Notch Filter and Capacitor Voltage Feedforward Active Damping Techniques for LCL Grid-connected Converters. *IEEE Trans. Power Electron.* **2019**, *34*, 3958–3972. [CrossRef]
17. Kang, L.Y.; Zhang, J.B.; Zhou, H.L. Model Predictive Current Control with Fixed Switching Frequency and Dead-time Compensation for Single-phase PWM Rectifier. *Electronics* **2021**, *10*, 426. [CrossRef]
18. An, Q.T.; Zhang, J.Q.; An, Q. Quasi-proportional-resonant Controller Based Adaptive Position Observer for Sensorless Control of PMSM Drives under Low Carrier Ratio. *IEEE Trans. Ind. Electron.* **2020**, *67*, 2564–2573. [CrossRef]
19. Peña-Alzola, R.; Liserre, M.; Blaabjerg, F.; Ordonez, M.; Yang, Y. LCL-filter Design for Robust Active Damping in Grid-connected Converters. *IEEE Trans. Ind. Inform.* **2014**, *10*, 2192–2203. [CrossRef]

20. Bao, C.L.; Ruan, X.B.; Wang, X.H.; Li, W.W.; Pan, D.H.; Weng, K. Step-by-Step Controller Design for LCL-type Grid-connected Inverter with Capacitor Current Feedback Active Damping. *IEEE Trans. Power Electron.* **2014**, *29*, 1239–1253.

21. Pan, D.H.; Ruan, X.B.; Bao, C.L.; Li, W.W.; Wang, X.H. Optimized Controller Design for LCL-type Grid-connected Inverter to Achieve High Robustness Against Grid-impedance Variation. *IEEE Trans. Ind. Electron.* **2015**, *62*, 1537–1547. [CrossRef]

22. Wang, X.; Blaabjerg, F.; Loh, P.C. Grid Current Feedback Active Damping for LCL Resonance in Grid-connected Voltage-source Converters. *IEEE Trans. Power Electron.* **2016**, *31*, 213–223. [CrossRef]

23. Xu, J.M.; Xie, S.J.; Tang, T. Active Damping-based Control for Grid-connected LCL-filtered Inverter with Injected Grid Current Feedback Only. *IEEE Trans. Ind. Electron.* **2014**, *1*, 4746–4758. [CrossRef]

24. Liu, H.Y.; Xu, D.G.; Li, L.; Gao, Q. Robust Damping Method for Voltage Source Converter with LCL-type Filter Under Weak Grid Conditions. *CSEE J. Power Energy Syst.* **2022**, *1*, 1428–1437.